

Channel Measurements and Modeling for 400–600-MHz Bands in Urban and Suburban Scenarios

Jie Huang¹, Member, IEEE, Cheng-Xiang Wang², Fellow, IEEE, Yuqian Yang, Yu Liu³, Member, IEEE, Jian Sun⁴, Member, IEEE, and Wensheng Zhang⁵, Member, IEEE

Abstract—Sub-1 GHz bands have been used for many years and now some of them will be reallocated for new applications, including the fifth generation (5G) wireless communication systems and beyond, Internet of Things (IoT), smart grid, etc. As the well-known path-loss (PL) models are mainly applicable in 2–6-GHz frequency range, a new channel measurement campaign is needed to study the propagation characteristics at sub-1 GHz bands. In this article, we conduct fixed-to-mobile wideband channel measurements at 400–600-MHz bands in urban and suburban scenarios using the time domain channel sounder. As the interference and noise signals are severe, the transmitted waveform is carefully designed to enlarge the system dynamic range. Meanwhile, ray tracing simulation is applied to construct the measurement environments and do the mutual verification with measurement results. The two-slope PL model and lognormal shadowing fading model are proposed for large-scale fading channel modeling. The root mean square (RMS) delay spread (DS), number of paths, and diffraction characteristics are also analyzed. The results will have great importance for the coming new applications at sub-1 GHz bands.

Index Terms—Channel measurements, channel modeling, ray tracing, sub-1 GHz bands, urban and suburban scenarios.

Manuscript received May 17, 2020; revised July 28, 2020 and September 18, 2020; accepted October 8, 2020. Date of publication October 20, 2020; date of current version March 24, 2021. This work was supported in part by the National Key Research and Development Program of China under Grant 2018YFB1801101; in part by the National Natural Science Foundation of China under Grant 61901109 and Grant 61960206006; in part by the Xinwei Project under Grant 11170011131701; in part by the National Postdoctoral Program for Innovative Talents under Grant BX20180062; in part by the Frontiers Science Center for Mobile Information Communication and Security; in part by the High Level Innovation and Entrepreneurial Research Team Program in Jiangsu; in part by the High Level Innovation and Entrepreneurial Talent Introduction Program in Jiangsu; in part by the Research Fund of National Mobile Communications Research Laboratory, Southeast University, under Grant 2020B01; in part by the Fundamental Research Funds for the Central Universities under Grant 2242020R30001; in part by the EU H2020 RISE TESTBED2 Project under Grant 872172; and in part by the Taishan Scholar Program of Shandong Province. (Corresponding author: Cheng-Xiang Wang.)

Jie Huang and Cheng-Xiang Wang are with the National Mobile Communications Research Laboratory, School of Information Science and Engineering, Southeast University, Nanjing 210096, China, and also with Pervasive Communication Research Center, Purple Mountain Laboratories, Nanjing 211111, China (e-mail: j_huang@seu.edu.cn; chxwang@seu.edu.cn).

Yuqian Yang, Jian Sun, and Wensheng Zhang are with the Shandong Provincial Key Laboratory of Wireless Communication Technologies, School of Information Science and Engineering, Shandong University, Qingdao 266237, China (e-mail: yangyuqianworking@126.com; sunjian@sdu.edu.cn; zhangwsh@sdu.edu.cn).

Yu Liu is with the School of Microelectronics, Shandong University, Jinan 250101, China (e-mail: yuliu@sdu.edu.cn).

Digital Object Identifier 10.1109/JIOT.2020.3032615

I. INTRODUCTION

IN PREVIOUS wireless communication systems, ultra high frequency (UHF) bands, such as 900/1800 MHz and 2.4 GHz have widely been used. Most channel measurements conducted at these bands are based on continuous wave (CW) or narrowband signal, such as the measurements in [1]–[3]. Properties of radio wave propagation above 400 MHz was reviewed in [4] with results only applied to narrowband. For wideband channel measurements, there exists some challenges. Since various communication systems and electronic devices are deployed in the environments, interference signals can have large effects on channel measurements. Meanwhile, the noise powers for wideband channel sounding are much higher than that of narrowband case, which degrades the system dynamic range.

Although the fifth generation (5G) and beyond communication systems explore higher frequency bands above 6 GHz, such as millimeter wave (mmWave) [5]–[9], terahertz (THz), and optical frequency bands [10]–[12], there is another trend to utilize the lower frequency bands, especially the sub-1 GHz bands. The sub-1 GHz bands have been used for many years and now some of them will be reallocated for many new applications, including 5G and beyond communication systems, Internet of Things (IoT) [13], [14], smart grid [15], etc. As the frequency is low, it benefits from favourable propagation characteristics and can be used for wide area coverage, high-speed scenarios, and massive device connections with low costs. Meanwhile, the sub-1 GHz bands can be used for emergency communications, such as telecommunication services for disaster relief and emergency telecommunication services [16]. By using sub-1 GHz bands, emergency communication services can be provided with high quality and flexibility during nature disasters and network outages.

The sub-1 GHz spectrum mainly comes from the digital dividend after digital television (TV) transition and currently deployed communication systems. For example, the 470–862-MHz band has widely been used for TV broadcast [17]. The 470–960-MHz band was allocated by International Telecommunication Union (ITU) on WRC-15 for terrestrial broadcasting and mobile services [13]. IEEE 802.11ah was developed to define sub-1 GHz license-exempt operation to provide extended range WiFi networks and support sensors and IoT applications [18], [19]. IEEE also released a white paper to use sub-1 GHz bands for smart

grid [20]. Groupe spécial mobile association (GSMA) planed to use sub-1 GHz for widespread coverage across urban, suburban, and rural areas, as well as IoT services [21]. In America, Federal Communications Commission (FCC) conducted an incentive auction to repurpose the 600-MHz band (614–698 MHz) in March 2017, yielding \$19.8 billion in revenue. T-Mobile rolled out a 5G network in 2019 using 617–652-MHz band for downlink and 663–698-MHz band for uplink to achieve nationwide coverage, and extended its network after completing merger with Sprint in 2020. In China, the 450–470-MHz band was evaluated to be used for the LTE-R railway communication system. The 600 and 700 MHz bands are also being considered for 5G in China.

Only a few channel measurements have been conducted at sub-1 GHz bands for the coming applications in the literature. In [22], a channel model was proposed for train to train communication at 400-MHz band. In [23] and [24], channel measurements were conducted at 700-MHz band for dedicated short-range communication (DSRC) in vehicular communication environments. In [25], outdoor channel measurements at 300-MHz band were conducted to validate the COST 2100 channel model. In [26], the 400-MHz band was used for implanted devices in the wireless body area network (WBAN). In [27], the 370-MHz band was studied for IoT communications. In [28], channel measurements were conducted on train stations of high-speed railways at 930 MHz. Several propagation characteristics, including large-scale fading and small-scale fading were studied. In [29], a channel model was proposed for suburban and rural environments at 450-MHz band. In [30], channel measurements were conducted in factory environments at 928.2 MHz. Different configurations with and without moving workers and metal machines were measured. The K factor was found to be smaller when the number of moving reflectors was high. In [31], channel measurements were conducted for LoRa wireless sensor links at 434 and 868 MHz in the Antarctic. The signal-to-noise ratio (SNR) and packet loss were analyzed. In [32], channel measurements were conducted at 921.6 MHz for low-power wide-area network. The theoretical received signal strength indicator (RSSI) based on the Okumura-Hata model was shown to be lower than the measured values. In [33], channel measurements were conducted for a body-to-body LoRa link at 868 MHz. The results showed that communication was reliable for a range over 500 m and over 200 m with the antennas pointed toward and away from each other, respectively.

The above-mentioned channel measurements are conducted with limited bandwidth. The wideband effects, such as the amplitude, delay, and angle parameters of multipath components (MPCs) are not fully characterized. Meanwhile, the well-known path-loss (PL) models are mainly applicable in 2–6-GHz frequency range. Thus, a new wideband channel measurement campaign is needed to study the propagation characteristics at sub-1 GHz bands. In this article, we aim to conduct fixed-to-mobile wideband channel measurements and modeling at 400–600-MHz bands in urban and suburban scenarios. To the best of our knowledge, it is the first wideband channel measurements and modeling at 400–600-MHz bands. The main contributions and novelties include as follows.

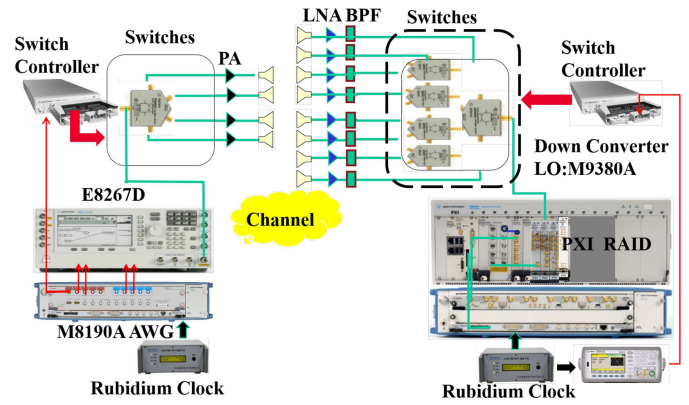


Fig. 1. Time-domain channel sounder.

- 1) The 400–600-MHz fixed-to-mobile wideband channel measurements are conducted in urban and suburban scenarios. The transmitted waveform is carefully designed to enlarge the system dynamic range of the time-domain channel sounder.
- 2) Ray tracing simulation is applied to construct the measurement environments and do the mutual verification with measurement results.
- 3) The two-slope PL model and lognormal shadowing fading model are proposed for large-scale channel modeling. Model parameters are obtained for both channel measurements and ray tracing simulations.
- 4) Important small-scale channel statistical properties, including the root mean square (RMS) delay spread (DS), number of paths, and diffraction characteristics are also analyzed.

The remainder of this article is organized as follows. Section II describes the channel sounder design, transmit waveform design and data processing, and channel measurement campaigns. In Section III, ray tracing simulation and the proposed PL model are given. The measurement and simulation results and analysis are presented in Section IV. Finally, the conclusions are drawn in Section V.

II. 400–600-MHz FIXED-TO-MOBILE WIDEBAND CHANNEL MEASUREMENTS

A. Channel Sounder Design

As shown in Fig. 1, the Keysight time-domain channel sounder is used to conduct fixed-to-mobile wideband channel measurements in outdoor environments. The 400–600-MHz bands are measured, i.e., the center frequency is 500 MHz and the bandwidth is 200 MHz. The transmitter (Tx) side consists of an M8190A arbitrary waveform generator (AWG) with sampling rate of 12 GSa/s, an E8267D vector signal generator (VSG) with frequency range of 100 kHz–44 GHz, an L4450A high-speed switch controller, a GPS Rubidium clock, and a Tx omnidirectional antenna. The receiver (Rx) side consists of an M9362A PXIe down converter, an M9352A PXI hybrid amplifier/attenuator, an M9300A PXIe frequency reference, an M9703B AXIe 12-b digitizer, an E8257D analog signal generator, an L4450A high speed switch controller, a GPS Rubidium

TABLE I
LIST OF EQUIPMENT FOR OUTDOOR CHANNEL MEASUREMENTS

Equipment	Main parameters	Usage
Channel sounder	Frequency range: 100 kHz–44 GHz, sampling rate: 12 GSa/s	Generate and save the measurement data
Tx/Rx antenna	Frequency range: 300 MHz–6 GHz, gain: 3 dBi, omnidirectional, elevation beamwidth: 60°	Transmit and receive wireless signals
PA/LNA	PA: 300–600 MHz, 40 dB gain, 38 dBm (+6 W) power, 24 V voltage; LNA: 10–700 MHz, 47 dB gain, 2 dB noise floor, 15 V voltage	Amplify the transmitted and received signals
Gasoline generator	Power: 3 kW, weight: 47 kg	Supply power for channel sounder
Extension reel	Power: 4 kW, length: 30 m	Extend the distance between power supply and channel sounder
Direct current power supply	Voltage: 30 V	Provide power for PA and LNA
Lifting gas rod	Height: 10 m	Lift the antenna up
Pickup trunk	Size: 5.3 m × 1.7 m × 1.7 m	Move the channel sounder

clock, and a Rx omnidirectional antenna. The omnidirectional antenna is working in the range of 300 MHz–6 GHz with antenna gain of 3 dBi and elevation beamwidth of 60°. The Rubidium clocks at Tx and Rx sides are utilized to synchronize the 1 pulse per second (PPS) signal with the coordinated universal time (UTC) from GPS satellite. To enlarge the dynamic range of the measurement system, the power amplifier (PA) and low noise amplifier (LNA) are connected near to the Tx and Rx antennas, respectively.

To conduct outdoor channel measurements, many practical problems should be taken into account, such as the measurable distance, movement/fix/charge of the measurement system, and interferences from the environment [34]. Thus, additional equipments are indispensable. A summary of the equipments used in channel measurements is given in Table I with their main parameters and usages.

In measurements, the Tx side is fixed and the Tx antenna is elevated to a height of 10 m above the floor using the lifting gas rod. The Rx side is moving in the measurement environments by the pickup trunk and the Rx antenna is fixed with a height of 3 m. Note that as the Rx sounder is put on the pickup trunk to move in the environment and we also need a tripod to fix the Rx antenna, it is not able to set its height at 1.6–1.8 m, which is the usual case. Otherwise, the signal will be largely blocked by the sounder and pickup trunk. At the Tx side, the self-designed wideband waveform is loaded to M8190A, then the wideband difference IQ signal is modulated to the carrier frequency by E8267D. The signal is transmitted through the cable, PA, and Tx antenna. At the Rx side, the fading signal is received through the Rx antenna, LNA, and the cable. Then, the received signal goes to M9362A and down converted to the intermediate frequency (IF) by the local oscillator (LO) provided by E8257D. The IF signal is then converted from analog to digital by M9703B, and then the

TABLE II
DEPLOYED COMMUNICATION SYSTEMS AT 400–600-MHz BANDS

System	Frequency band (MHz)
T-GSM-410	410.2–419.8 (uplink), 420.2–429.8 (downlink)
GSM-450	450.4–457.6 (uplink), 460.4–467.6 (downlink)
GSM-480	478.8–486 (uplink), 488.8–496 (downlink)
TETRA	410–420/450–460 (uplink), 420–430/460–470 (downlink)
LED D2D	452.5–457.5 (uplink), 462.5–467.5 (downlink)
ZigBee (IEEE 802.15.4)	250–750
NFC/RFID	433
Broadband services in rural and remote areas	450–470
Digital TV broadcast	470–806
Amateur radio	430–440

baseband IQ signal is obtained from orthogonal demodulation. The measurement system is autocontrolled by software programs at both sides. The signal frequency, sampling rate, signal waveform, and waveform length can be configured at the Tx side, and the signal frequency, signal bandwidth, waveform length, recording waveform length, and file name can be configured at the Rx side.

B. Transmit Waveform Design and Data Processing

Preliminary measurements indicate that there are many interference signals at 400–600-MHz bands due to the various deployed communication systems, as shown in Table II. The interference signals will have large effects on channel measurements, which make the wideband channel measurements a challenging task.

To enlarge the system dynamic range, a high-order pseudonoise (PN) sequence with length up to $2^{20} = 1048576$ is used to obtain processing gain of $10\log_{10}2^{20} = 60$ dB. In addition, 7000 zero points and 1424 cyclic prefix (CP) are added at the start of the waveform. To further reduce the intersymbol interference (ISI), the transmitted waveform is interpolated with four times and filtered by a root raised cosine (RRC) pulse shaping filter with roll-off factor of 0.25. The received signal is then filtered by using the same matched RRC filter and downsampled.

Let us denote the transmit signal as $x(t)$, the response of the measurement system and PA as $g(t)$, and the channel impulse response (CIR) as $h(t)$. The back-to-back calibration signal is

$$y_{th}(t) = x(t) * g(t) \quad (1)$$

where $*$ is the convolution operation. In the time domain, the received wireless signal is the convolution of the transmit signal, CIR, and system response. Thus, the received signal is expressed as

$$y_{rx}(t) = x(t) * g(t) * h(t). \quad (2)$$

The frequency-domain response can be obtained from the Fourier transform of the time-domain response. The frequency-domain calibration signal and received wireless signal are given as

$$Y_{th}(f) = X(f)G(f) \quad (3)$$

$$Y_{rx}(f) = X(f)G(f)H(f). \quad (4)$$

The CIR is then obtained from the inverse Fourier transform of the frequency-domain response. It is expressed as

$$h(t) = \text{IFFT}(H(f)) = \text{IFFT}(Y_{rx}(f)/Y_{th}(f)). \quad (5)$$

For each calibrated CIR, the peak search algorithm is applied to extract MPCs in delay domain from the measured power delay profile (PDP). Specifically, the peak search algorithm includes four steps.

- 1) *Step 1*: Calculate the maximum received power P_{max} (in dB) and average noise floor N_{ave} (in dB).
- 2) *Step 2*: Define the length of the measured PDP as K . For delay index $k = 2, \dots, K - 1$, if $\text{PDP}(k)$ (in linear) is greater than its adjacent elements, output its position index (k) and value ($\text{PDP}(k)$).
- 3) *Step 3*: If $10\log_{10}(\text{PDP}(k)) < \max(P_{max} - 40, N_{ave} + 10)$, this data point is discarded.
- 4) *Step 4*: If the number of output points is greater than the predefined number of significant maxima 100, just select the strongest 100 points.

The received power is the summation of the power of each MPC, i.e.,

$$P = 10\log_{10}\left(\sum_{l=1}^L P_l\right) \quad (6)$$

where L is the number of MPCs and P_l is the power of the l th path in linear. Note that L is less than or equal to 100. Later, we will see from the results on the number of paths in urban and suburban scenarios that the probability of more than 100 paths is nearly zero. Thus, the number 100 is reasonable and sufficient to take all paths into account.

After the calibration of antennas and LNA, the PL caused by the wireless channel is obtained. It is expressed as

$$\text{PL}(\text{dB}) = -P + G_t + G_r + G_{\text{LNA}} \quad (7)$$

where G_t (3 dB), G_r (3 dB), and G_{LNA} (47 dB) are the gains of the Tx antenna, Rx antenna, and LNA, respectively. Note that the gain of PA is included in the back-to-back calibration. The RMS DS is an important second-order statistic property and calculated as

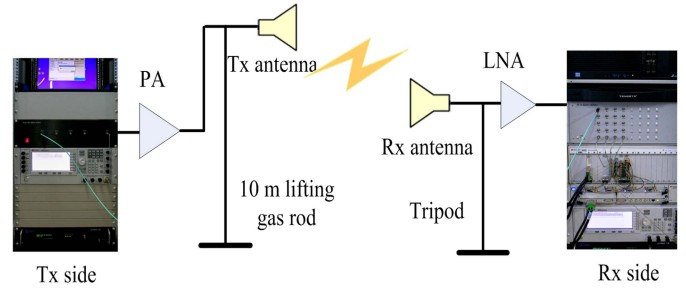
$$\text{DS} = \sqrt{\frac{\sum_{l=1}^L P_l \tau_l^2}{\sum_{l=1}^L P_l} - \left(\frac{\sum_{l=1}^L P_l \tau_l}{\sum_{l=1}^L P_l}\right)^2} \quad (8)$$

where τ_l is the delay of the l th path.

C. Wideband Channel Measurements

The wideband channel measurements are conducted at 400–600-MHz bands in urban and suburban scenarios. An illustration of the measurement set up and measurement procedures are shown in Fig. 2. At first, we set up the channel sounder, PA/LNA, and antennas at Tx and Rx sides. Then, a back-to-back calibration is conducted to calibrate out the system response from the channel sounder. After that, we move the Rx sounder by the pickup truck and collect measurement data. Finally, the measurement data are processed and analyzed.

Note that in our measurements, the measured delay is the relative delay rather than the absolute delay. It is not feasible to



- Step1: Set up the channel sounder, PA/LNA, and antennas at Tx and Rx sides
- Step2: Conduct the back-to-back calibration
- Step3: Move the Rx sounder by the pickup truck and collect measurement data
- Step4: Process and analyze the measurement data

Fig. 2. Illustration of the measurement set up and measurement procedure.

identify the line-of-sight (LOS) and non line-of-sight (NLOS) cases from the measurement data automatically. Thus, the measurement results presented here is a combination of LOS and NLOS measurement results. As the measurement environments are rich scattering at the measured frequency band, the LOS path would have less impact on the measured CIR.

In two scenarios, the Tx side is fixed with Tx antenna height of 10 m, while the Rx side is moving on a pickup truck with Rx antenna height of 3 m, as shown in Figs. 3 and 4. The Rx speed varies with the traffic flow and rule in the measurement environment and it is 30 km/h in average. For urban scenario, channel measurements are conducted around central campus of Shandong University, Jinan, China. The Tx is located near the south entrance on Shanda South Road with coordinate (N36.6719°, E117.0601°). For the suburban scenario, channel measurements are conducted in the area of Shayi village to Shasan village, Wangsheren town, Jinan, China. The Tx is located near the entrance of Sha'er village with coordinate (N36.7536°, E117.1310°).

For the urban scenario, the buildings are high and dense with heights in the range of 6–50 m. Trees at roadsides are about 8–10 m height. The road width is about 10–20 m with four vehicle lanes, bicycle lane, and sidewalk. The vehicle and human traffics are heavy and the interferences and noises are severe. The movement of Rx pickup should obey traffic rules.

For the suburban scenario, the buildings are in the height of 5–10 m with one to three floors. The road is relatively narrow with main road width of 6 m and side road width of 3 m. The traffic density and interference and noises are relatively lower. The movement of Rx is more flexible.

Both the theoretical method and universal transverse Mercator (UTM) are used to calculate the distance between two coordinate points. The UTM is a system for assigning coordinates to locations on the surface of the Earth and has been widely used in geomorphology. Using the theoretical method, the distance between A ($\text{Lat}_A, \text{Lon}_A$) and B ($\text{Lat}_B, \text{Lon}_B$) can be calculated as

$$D = R \times \arccos(C) \quad (9)$$

$$C = \sin\left(\frac{\pi}{2} - \text{Lat}_A\right) \times \sin\left(\frac{\pi}{2} - \text{Lat}_B\right) \times \cos(\text{Lon}_A - \text{Lon}_B) + \cos\left(\frac{\pi}{2} - \text{Lat}_A\right) \times \cos\left(\frac{\pi}{2} - \text{Lat}_B\right) \quad (10)$$

where $R = 6371.004$ km is the average radius of the earth.



Fig. 3. Channel sounder set up in an urban scenario.



Fig. 4. Channel sounder set up in a suburban scenario.

The Rx trajectory on the network road map for urban and suburban scenarios is shown in Figs. 5 and 6, respectively. The Tx location is used as the original coordinate for distance calculation in the two scenarios. The Rx moves back and forth on the main roads. The maximum distance is 1500 and 800 m in urban and suburban scenarios, respectively. The Tx–Rx distance calculated by the two methods agree well with each other, as shown in Fig. 7.

III. 400–600-MHZ CHANNEL MODELING

A. Ray Tracing Simulation

The ray tracing simulation is completed by using Wireless Insite software. The constructed urban and suburban scenarios

are same with the measurement campaigns based on digital map database, as shown in Fig. 8. The simulated areas in urban and suburban scenarios are about 3×1.2 and 1.4×0.9 km², respectively.

The main parameters in ray tracing simulation are the same with channel measurements. Two omnidirectional antennas are used at Tx and Rx sides. The transmitted power is set as 0 dBm. The simulated frequency is centered at 500- with 200-MHz bandwidth. The maximum PL is set as 120 dB. Building materials are assumed to be concrete with permittivity of $\xi = 15$ F/m and conductivity of $\sigma = 0.015$ S/m. Vegetation effects are also taken into account. In the urban scenario, trees are set to be on the side of main roads with

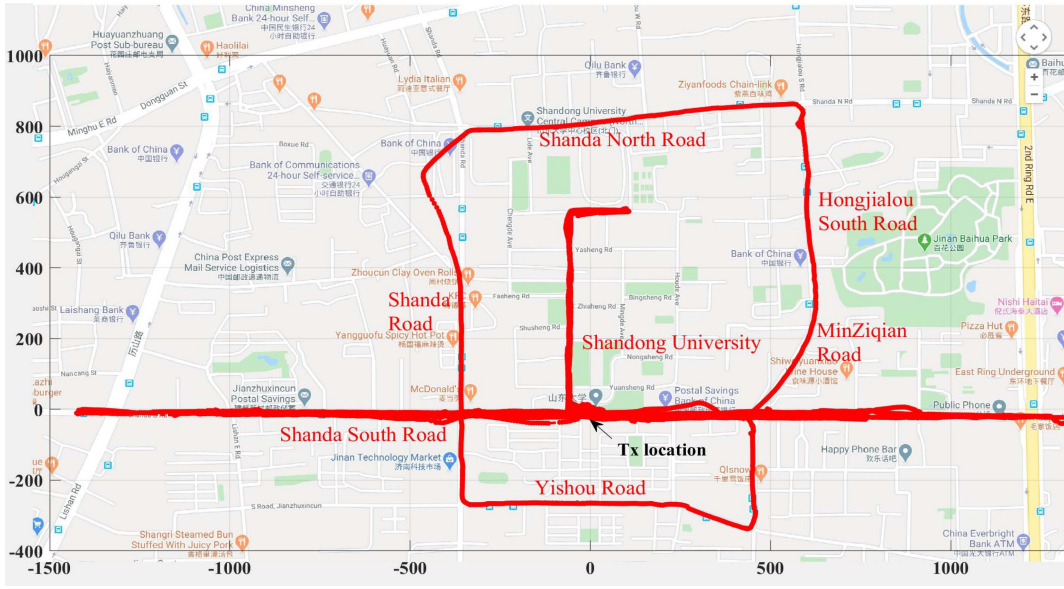


Fig. 5. Road network map and Rx trajectory in an urban scenario.

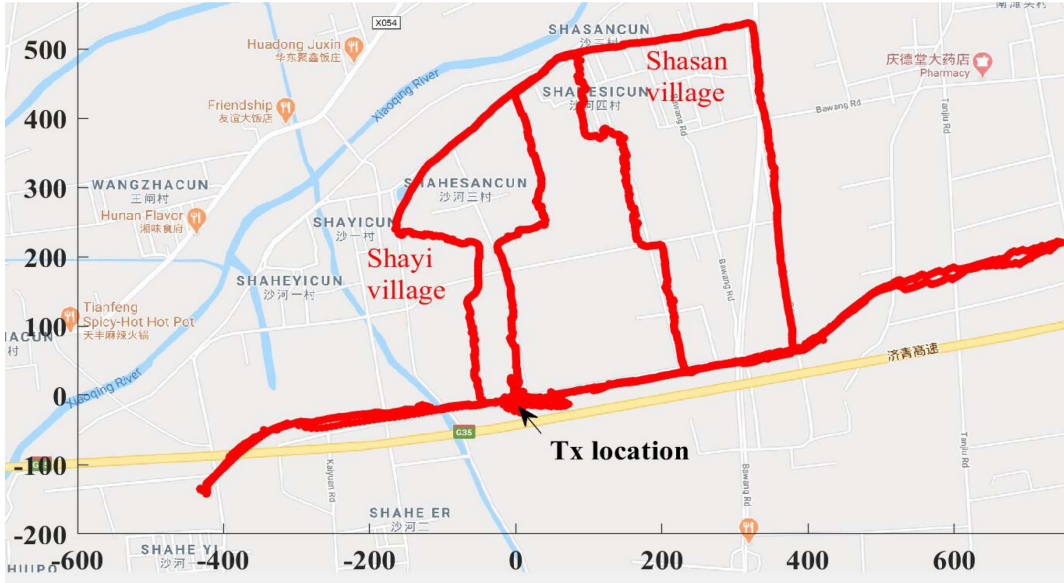


Fig. 6. Road network map and Rx trajectory in a suburban scenario.

height of 8 m. In a suburban scenario, there are several open lands on the side of main roads with height of 1.5 m. The Tx antenna is set at the same location and height with channel measurements. The Rx route is the same with channel measurements with 3-m distance separation between two sampling positions.

Up to third-order reflection and first-order diffraction are considered in the simulation. The received power is calculated as

$$P_r = \frac{P_t G_t G_r \lambda^2}{(4\pi d)^2} \left(\prod R_i \right)^2 \left(\prod A(s, s') D_j \right)^2 \quad (11)$$

where P_t is the transmitted power, λ is the wavelength, d is the Tx–Rx distance, R_i is the i th reflection coefficient, D_j is the j th diffraction coefficient, and $A(s, s')$ is the diffraction attenuation with s and s' denoting the distance from the diffraction point

to Rx and Tx, respectively. An illustration of the simulated MPCs in urban and suburban scenarios is shown in Fig. 9.

B. Path-Loss Models

Several PL models have widely been used, such as the Okumura-Hata model, COST-231 model, WINNER II model [35], 3GPP TR 38.901 model [36], 3GPP TR 38.901 model, and ITU-R M.2135 (IMT-A) model [37]. A summary of the Okumura-Hata, COST-231, 3GPP TR 36.873, and 3GPP TR 38.901 PL models is given in Table III, with their applicable frequency range f_c , heights of base station (BS) antenna (h_{BS}) and mobile station (MS) antenna (h_{MS}), Tx–Rx distance d , etc.

As can be seen, these PL models are not applicable to our measurement case. Thus, we try to propose a new PL model to

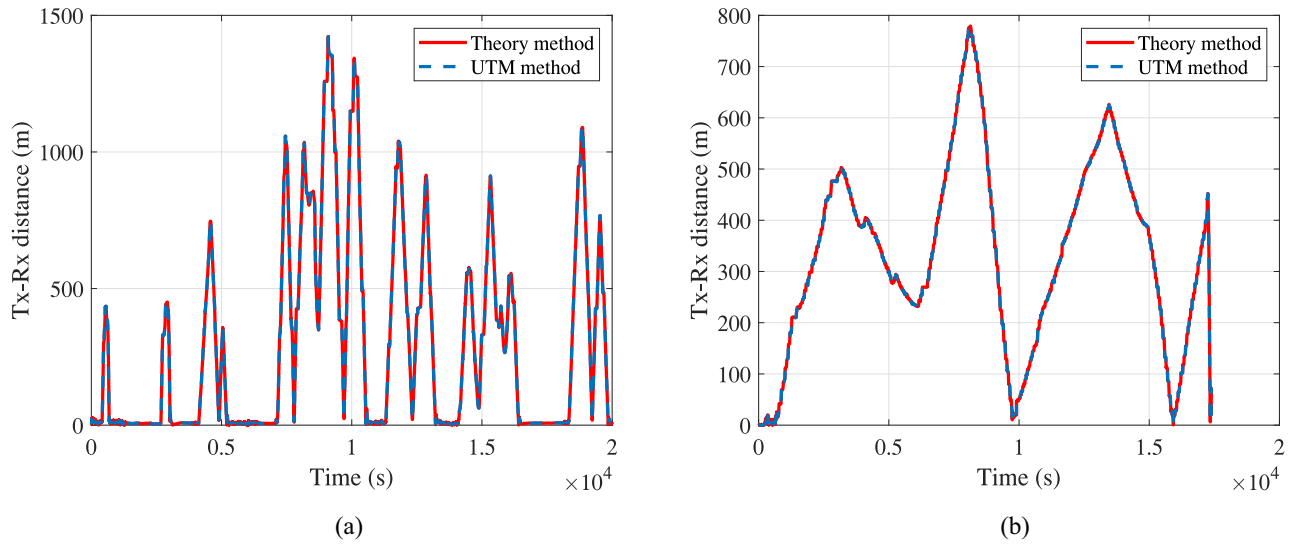


Fig. 7. Tx-Rx distances for (a) urban and (b) suburban scenarios.

 TABLE III
 SUMMARY OF THE OKUMURA-HATA, COST-231, 3GPP TR 38.901, AND 3GPP TR 38.901 PL MODELS

PL model	Application condition	Expression
Okumura-Hata	f_c : 150–1500 MHz, h_{BS} : 30–200 m, h_{MS} : 1–10 m, d : 1–35 km	$PL = 69.55 + 26.16\log_{10}(f_c) - 13.82\log_{10}(h_{BS}) + (44.9 - 6.55\log_{10}(h_{BS}))\log_{10}(d) - a(h_{MS})$ Urban: $a(h_{MS}) = (1.1\log_{10}(f_c) - 0.7)h_{MS} - (1.56\log_{10}(f_c) - 0.8)$ Suburban: $a(h_{MS}) = -2[\log_{10}(f_c/28)]^2 - 5.4$ Note: f_c in MHz, d in km
COST231-Hata	f_c : 1500–2000 MHz, h_{BS} : 30–200 m, h_{MS} : 1–10 m, d : 1–20 km	$PL = 46.3 + 33.9\log_{10}(f_c) - 13.82\log_{10}(h_{MS}) - a(h_{MS}) + (44.9 - 6.55\log_{10}(h_{MS}))\log_{10}(d)$ Note: f_c in MHz, d in km
3GPP TR 36.873	f_c : 2–6 GHz, h_{BS} : 25 m, h_{MS} : 1.5–22.5 m, d : 10–5000 m	Urban macro (UMa) LOS: $PL_{LOS} = \begin{cases} 22\log_{10}(d) + 28 + 20\log_{10}(f_c), & d < d_{BP} \\ 40\log_{10}(d) + 28 + 20\log_{10}(f_c) - 9\log_{10}(d_{BP}^2 + (h_{BS} - h_{MS})^2), & d > d_{BP} \end{cases}$ UMa NLOS: $PL = \max(PL_{NLOS}, PL_{LOS})$ $PL_{NLOS} = 161.04 - 7.1\log_{10}(W) + 7.5\log_{10}(h) - (24.37 - 3.7(h/h_{MS})^2)\log_{10}(h_{MS}) + (43.42 - 3.1\log_{10}(h_{BS}))(\log_{10}(d) - 3) + 20\log_{10}(f_c) - (3.2(\log_{10}(17.625))^2 - 4.97) - 0.6(h_{MS} - 1.5)$ Note: f_c in GHz, d in m, W is street width, h is average building height, standard deviation of shadowing fading is 4 dB and 6 dB in LOS and NLOS, respectively
3GPP TR 38.901	f_c : 0.5–100 GHz, h_{BS} : 25 m, h_{MS} : 1.5–22.5 m, d : 10–5000 m	UMa LOS: same with 3GPP TR 36.873 UMa NLOS: $PL = \max(PL_{NLOS}, PL_{LOS})$ $PL_{NLOS} = 13.54 + 39.08\log_{10}(d) + 20\log_{10}(f_c) - 0.6(h_{MS} - 1.5)$ Note: f_c in GHz, d in m, standard deviation of shadowing fading is 4 dB and 6 dB in LOS and NLOS, respectively

fit our measurement results. The proposed two-slope PL model is mainly based on 3GPP TR 36.873 model, which takes the Tx–Rx distance, frequency, and Tx and Rx antenna heights into account.

The proposed two-slope PL model is

$$PL = \begin{cases} 10n_1\log_{10}(d) + A_1 + 20\log_{10}(f_c), & d \leq d_{BP} \\ 10n_2\log_{10}(d) + A_2 + 20\log_{10}(f_c), & d > d_{BP} \end{cases} \quad (12)$$

where n_1 and A_1 are the PL exponent and fitting parameter before the break point, respectively, while n_2 and A_2 are the PL exponent and fitting parameter after the break point, respectively. The carrier frequency f_c is 500 MHz.

For the urban scenario, the break point distance is expressed as

$$d_{BP} = 4(h_{BS} - 1)(h_{MS} - 1)f_c/c \quad (13)$$

where h_{BS} is the height of BS (Tx) antenna, h_{MS} is the height of MS (Rx) antenna, and $c = 3 \times 10^8$ m/s is the speed of

light. For the suburban scenario, the break point distance is expressed as

$$d_{BP} = 4h_{BS}h_{MS}f_c/c. \quad (14)$$

In the urban scenario, the terms $h_{BS} - 1$ and $h_{MS} - 1$ are the effective antenna heights, as the enormous humans, vehicles, and other objects are assumed to have an effective environment height of 1 m. In the suburban scenario, the objects have a lower density and the break point distance is calculated from the real Tx and Rx antenna heights. The shadowing fading is then modeled as lognormal distribution with the mean value of 0 dB and standard deviation of σ_s dB.

IV. MEASUREMENT AND SIMULATION RESULTS AND ANALYSIS

A. Measurement Results and Analysis

As an example, Fig. 10 shows the measured PDP in urban and suburban scenarios. It is the averaged PDP over several



Fig. 8. Constructed (a) urban and (b) suburban scenarios using ray tracing.

snapshots. For each measurement PDP, the statistics, including threshold, number of paths, received power, RMS DS, and Tx-Rx 3-D distance, are given.

The measured path losses for urban and suburban scenarios are shown in Fig. 11. The measurement data are well fitted by the two-slope model. For the urban scenario, the break point distance is 120 m, while it is 200 m for the suburban scenario. As a comparison, the free space PL model and one-slope model are also plotted. Note that the results are for combined LOS and NLOS conditions. The probability of LOS propagation is about 30% in urban scenario and 18% in the suburban scenario in our measurement, respectively.

Table IV shows the parameter values of the proposed PL model. Before the break point, the PL exponent is less than 2, which indicates there are strong reflected paths to enhance the signal power. After the break point, the PL exponent is greater than 2, because the signal is blocked by the buildings, vegetations, and other objects in the environment. In the urban scenario, buildings are regularly distributed on grids and roads are wide, while the buildings are irregularly distributed and roads are narrow in the suburban scenario. Thus, the PL

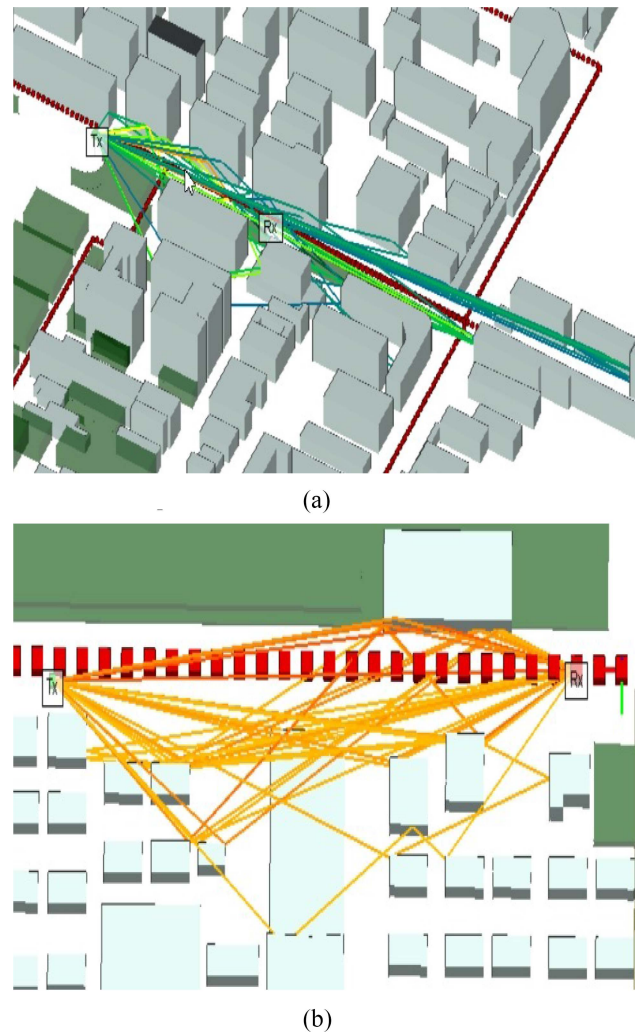


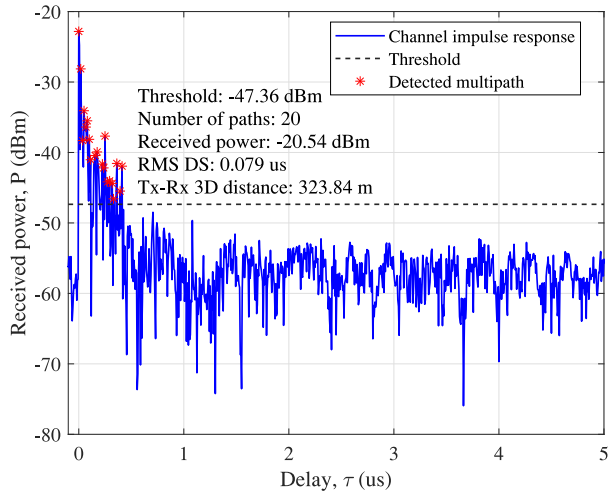
Fig. 9. Simulated MPCs in (a) urban and (b) suburban scenarios in a snapshot.

TABLE IV
MEASURED PL AND SHADOWING FADING PARAMETERS
FOR URBAN AND SUBURBAN SCENARIOS

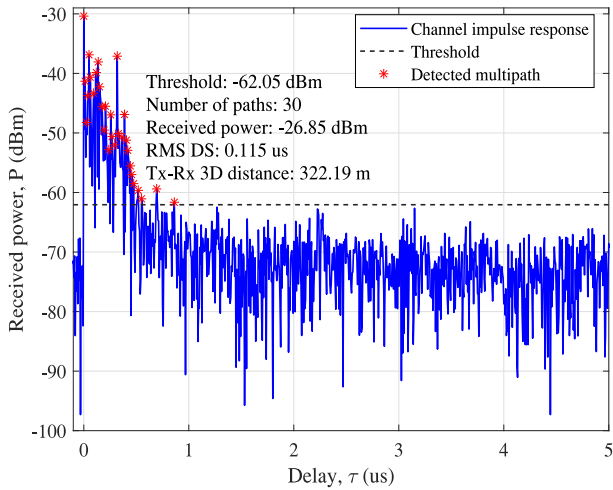
Scenario	Urban	Suburban
PL exponent	$n_1 = 0.10, n_2 = 5.24$	$n_1 = 1.47, n_2 = 6.42$
Fitting parameter	$A_1 = 62.42, A_2 = -44.20$	$A_1 = 37.54, A_2 = -71.70$
Standard deviation (dB)	3.03 (before), 7.40 (after)	6.63 (before), 9.22 (after)

exponent in a suburban scenario is slightly larger than that of urban scenario.

We also compare our measurement results with the existing models. In Okumura-Hata and COST231-Hata models, the PL exponent is related with the height of MS. In the 3GPP TR 36.873 model, the PL exponent is 2.2 and 4.0 in UMa LOS scenario before and after the break point, respectively. In the UMa NLOS case, the PL exponent is related with the height of BS. In the 3GPP TR 38.901 model, the PL exponent is set as 3.908 for UMa NLOS case. The standard deviation of shadowing fading is set as 4 and 6 dB in LOS and NLOS, respectively. In the above models, as the height of BS antenna is much higher than our measurements, the PL exponent and



(a)

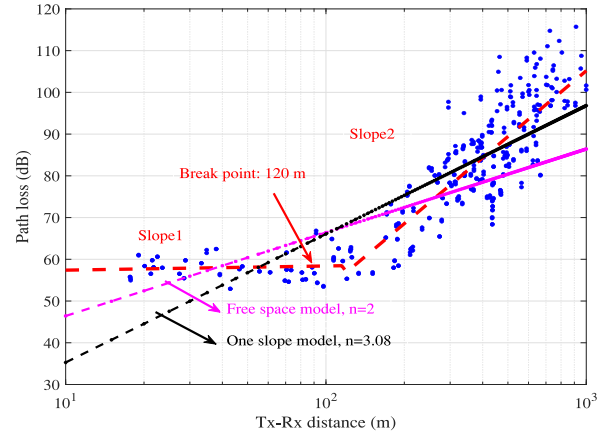


(b)

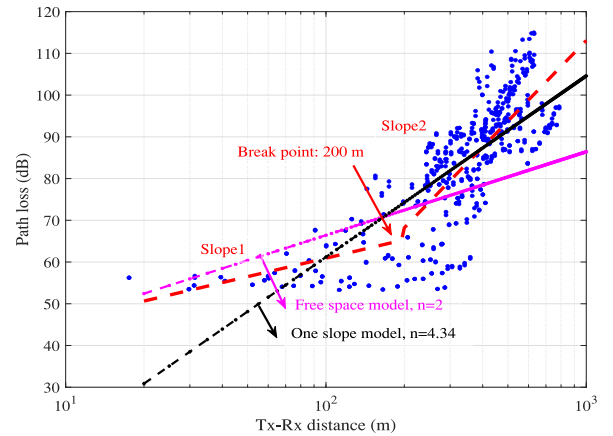
Fig. 10. Measured PDPs in (a) urban and (b) suburban scenarios.

shadowing fading are generally smaller than our measurement results. Our measurement results are comparable with [27], where wideband channel measurements were conducted for IoT applications in the range of 37.8–380 MHz. The PL exponent was in the range of 4.13–4.80, the shadowing fading was in the range of 8.87–10.96 dB.

Fig. 12 shows the cumulative distribution function (CDF) of RMS DS for urban scenario, while the CDF of RMS DS in suburban scenario is shown in Fig. 13. Note that the LOS and NLOS cases are clarified by using the GPS information and the map. For LOS conditions, the RMS DS is less than 2 us, while it can be 7 and 12 us for urban and suburban scenarios in NLOS conditions. The RMS DS in the urban scenario is less than that of the suburban scenario. The median RMS DS is 130 ns and 565 ns for urban and suburban scenario, respectively. In comparison, the measured median DS in [27] was found to increase with frequency and in the range of 250–750 ns when the frequency was in the range of 37.8–380 MHz.



(a)



(b)

Fig. 11. PL models for (a) urban and (b) suburban scenarios.

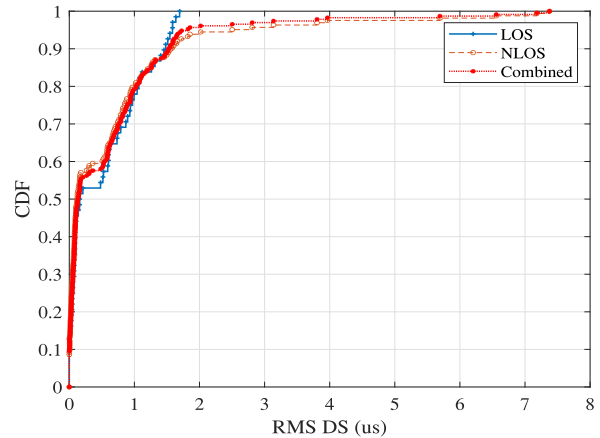


Fig. 12. CDF of RMS DS for an urban scenario.

Fig. 14 shows the probability density function (PDF) of the measured number of paths for urban and suburban scenarios. The Gaussian mixture model (GMM) is used to fit the PDF, with its PDF expressed as

$$p(x) = \sum_{i=1}^K \phi_i \frac{1}{\sqrt{2\pi\sigma_i^2}} e^{-\frac{(x-\mu_i)^2}{2\sigma_i^2}} \quad (15)$$

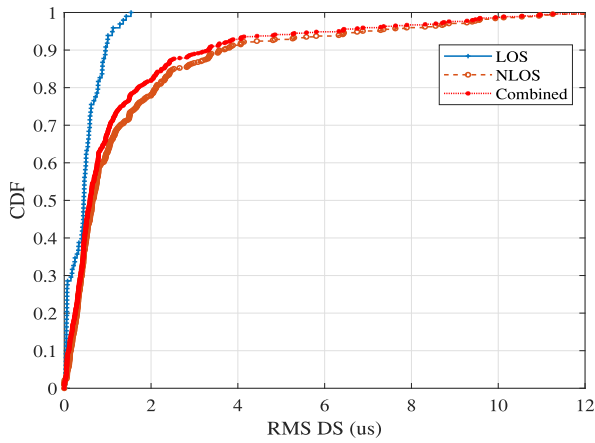
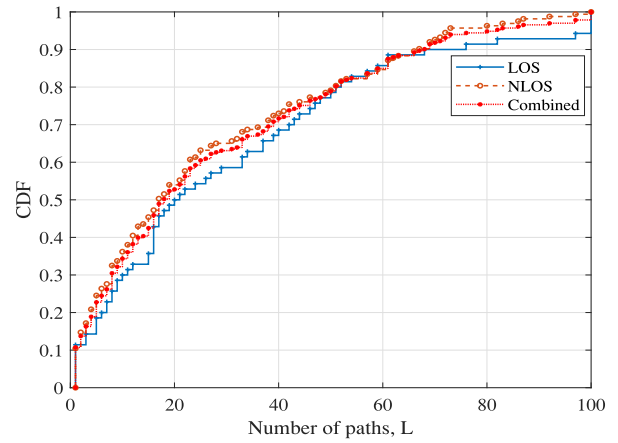
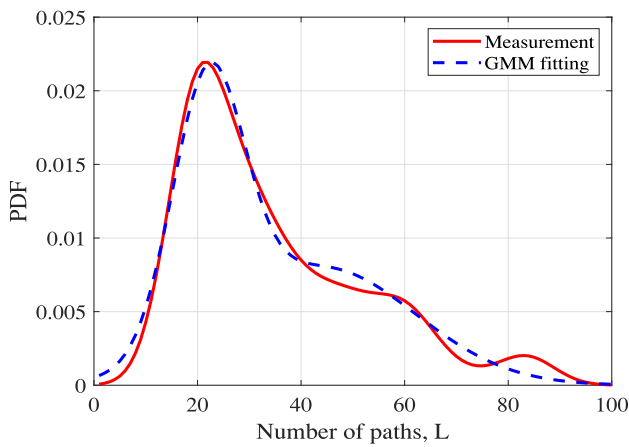


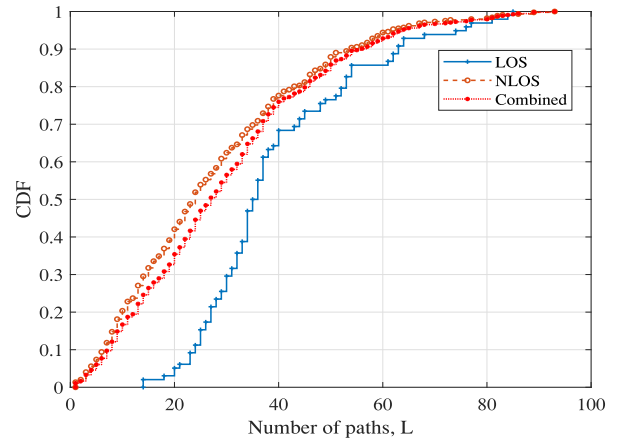
Fig. 13. CDF of RMS DS for a suburban scenario.



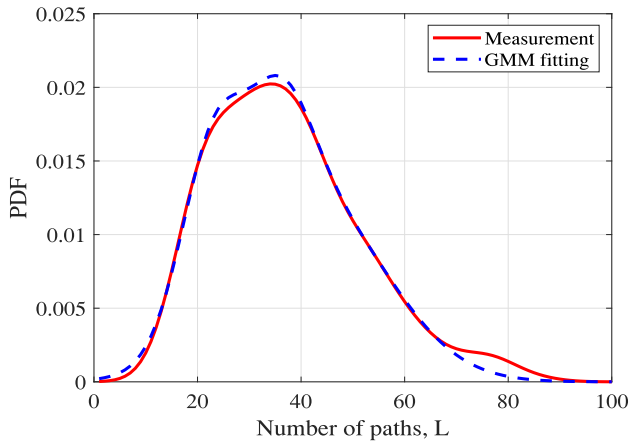
(a)



(a)



(b)



(b)

Fig. 14. Measured and fitted PDFs of numbers of paths for (a) urban and (b) suburban scenarios.

where the PDF is a combination of K Gaussian distributions with mean value and standard deviation of μ_i and σ_i , respectively, and with weight factor of ϕ_i .

In the urban scenario, the PDF of number of paths is fitted by two Gaussian distributions as $0.018N(22.04, 9.76^2) + 0.008N(43.95, 25.64^2)$. In the suburban scenario, the PDF

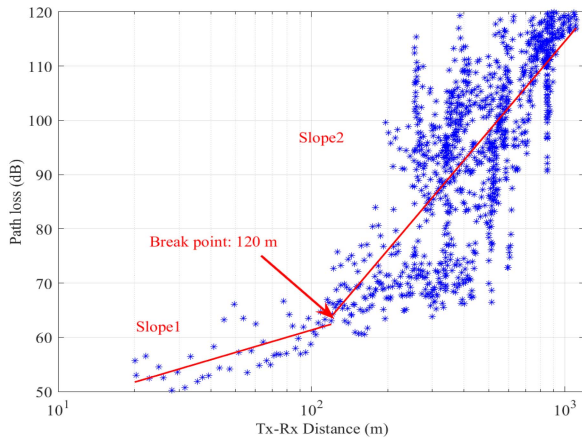
Fig. 15. Measured CDFs of numbers of paths for LOS and NLOS conditions in (a) urban and (b) suburban scenarios.

of number of paths is fitted by three Gaussian distributions as $-0.046N(29.26, 9.04^2) + 0.058N(28.94, 10.30^2) + 0.012N(42.33, 20.17^2)$. Fig. 15 shows the CDFs of the measured number of paths for LOS and NLOS conditions in urban and suburban scenarios. In comparison, urban scenario has a smaller number of paths, the number of paths in LOS condition is generally larger than that of NLOS condition.

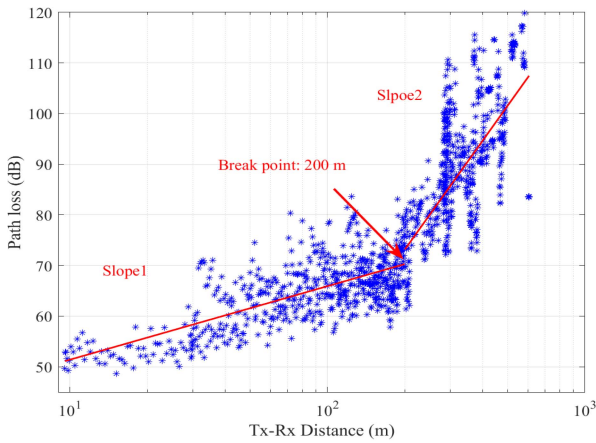
B. Simulation Results and Analysis

Fig. 16 shows the simulated PL for urban and suburban scenarios. The simulated PL also shows a clear two-slope behavior and the values are similar to the measurement results, as shown in Table V.

In addition, we study the diffraction effect around the crossroads and edge of buildings. We compare the propagation characteristics of two Rx positions before diffraction (Rx1) and after diffraction (Rx2). Fig. 17 shows the simulated PDPs. The received power at Rx1 and Rx2 are -68.96 and -80.60 dBm, respectively. The diffraction loss is about 12 dB. Before the diffraction, signal mainly comes from MPCs with small delays. After the diffraction, signal comes from MPCs with larger delays and the signal level is lower.



(a)



(b)

Fig. 16. Simulated PLs for (a) urban and (b) suburban scenarios.

TABLE V
SIMULATED PL AND SHADOWING FADING PARAMETERS FOR URBAN AND SUBURBAN SCENARIOS

Scenario	Urban	Suburban
PL exponent	$n_1 = 1.38, n_2 = 5.50$	$n_1 = 1.44, n_2 = 6.87$
Fitting parameter	$A_1 = 44.10, A_2 = -33.02$	$A_1 = 42.80, A_2 = -74.30$
Standard deviation (dB)	3.50 (before), 11.21 (after)	4.96 (before), 8.85 (after)

Fig. 18 shows the angle of arrival and angle of departure for Rx1 and Rx2. As can be seen, the distribution of angle of departure is similar for Rx1 and Rx2. However, as the diffraction has an effect on the received power of the signal, the angle of arrival has a large difference. Before the diffraction, the angles comes from several clusters. After the diffraction, the angle has a large dispersion due to the random effect of diffraction.

V. CONCLUSIONS

In this article, we have conducted fixed-to-mobile wideband channel measurements at 400–600-MHz bands in urban and suburban scenarios. By carefully designing the transmit waveform and the use of high performance PA and LNA,

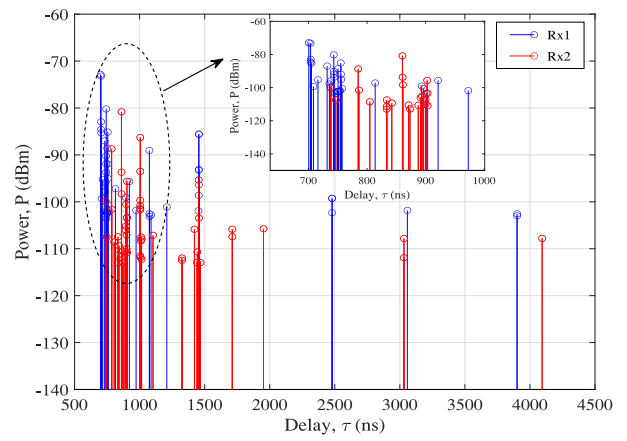
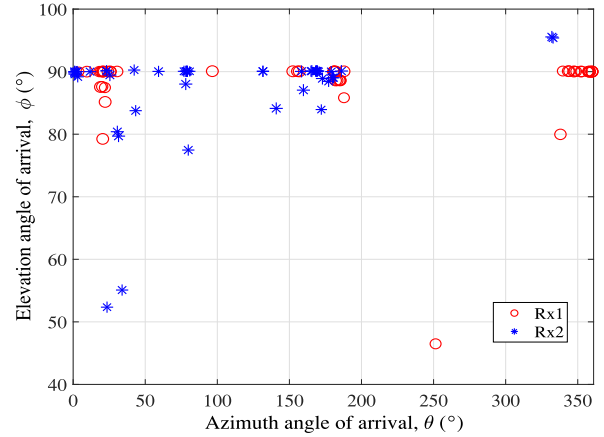
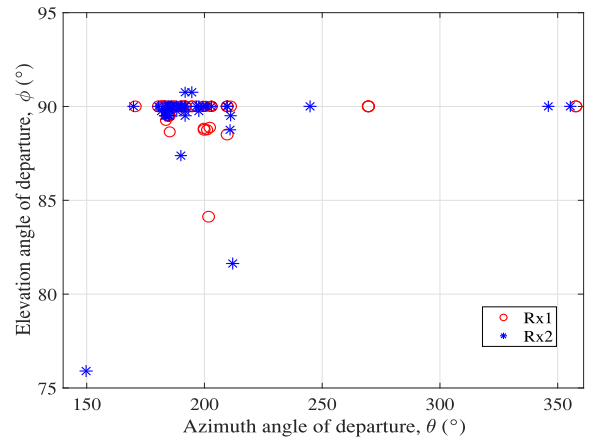


Fig. 17. Simulated PDPs before and after diffraction.



(a)



(b)

Fig. 18. Simulated (a) angles of arrival and (b) angles of departure for Rx1 and Rx2.

we have been able to enlarge the system dynamic range and do wideband channel measurements in this frequency band. The measurement results agree with the ray tracing simulation results, which mutually validates the measurement and simulation procedures. The two-slope PL model is found to be applicable. The PL exponent in the urban scenario is smaller than that in the suburban scenario, being 5.24 and 6.42 after the break point, respectively. The shadowing fading in urban

scenario is also smaller than that in suburban scenario. The median of RMS DS is 130 ns in urban scenario, while it is 565 ns in suburban scenario. The mean number of paths is 22 in urban scenario, while it is 34 in suburban scenario. In summary, the urban scenario is shown to have smaller RMS DS and number of paths, as well as a smaller break point distance. The diffraction can cause a power loss up to 12 dB. The results will be important for the coming new applications at sub-1 GHz bands.

ACKNOWLEDGMENT

The authors would like to acknowledge Hengtai Chang, Dewen Li, and Haodong Li from Shandong University, and Ji Bian from Shandong Normal University for their help in the channel measurements.

REFERENCES

- [1] J. H. Whitteker, "Measurements of path loss at 910 MHz for proposed microcell urban mobile systems," *IEEE Trans. Veh. Technol.*, vol. 37, no. 3, pp. 125–129, Aug. 1988.
- [2] J.-E. Berg, R. Bownds, and F. Lotse, "Path loss and fading models for microcells at 900 MHz," in *Proc. Veh. Technol. Soc. 42nd VTS Conf. Front. Technol. (VTC)*, Denver, CO, USA, 1992, pp. 666–671.
- [3] T. R. Rao, S. V. Rao, M. Prasad, M. Sain, A. Iqbal, and D. R. Lakshmi, "Mobile radio propagation path loss studies at VHF/UHF bands in southern India," *IEEE Trans. Broadcast.*, vol. 46, no. 2, pp. 158–164, Jun. 2000.
- [4] D. O. Reudink, "Properties of mobile radio propagation above 400 MHz," *IEEE Trans. Veh. Technol.*, vol. 23, no. 4, pp. 143–159, Nov. 1974.
- [5] J. Huang, C.-X. Wang, R. Feng, J. Sun, W. Zhang, and Y. Yang, "Multi-frequency mmWave massive MIMO channel measurements and characterization for 5G wireless communication systems," *IEEE J. Sel. Areas Commun.*, vol. 35, no. 7, pp. 1591–1605, Jul. 2017.
- [6] J. Zhang, P. Tang, L. Tian, Z. Hu, T. Wang, and H. Wang, "6–100 GHz research progress and challenges from a channel perspective for fifth generation (5G) and future wireless communication," *Sci. China Inf. Sci.*, vol. 60, no. 8, pp. 1–18, Aug. 2017.
- [7] X. Wu *et al.*, "60-GHz millimeter-wave channel measurements and modeling for indoor office environments," *IEEE Trans. Antennas Propag.*, vol. 65, no. 4, pp. 1912–1924, Apr. 2017.
- [8] J. Huang, C.-X. Wang, Y. Liu, J. Sun, and W. Zhang, "A novel 3D GBBSM for mmWave MIMO channels," *Sci. China Inf. Sci.*, vol. 61, no. 10, pp. 1–15, Oct. 2018.
- [9] J. Huang, Y. Liu, C.-X. Wang, J. Sun, and H. Xiao, "5G millimeter wave channel sounders, measurements, and models: Recent developments and future challenges," *IEEE Commun. Mag.*, vol. 57, no. 1, pp. 138–145, Jan. 2019.
- [10] C.-X. Wang *et al.*, "Cellular architecture and key technologies for 5G wireless communication networks," *IEEE Commun. Mag.*, vol. 52, no. 2, pp. 122–130, Feb. 2014.
- [11] S. Wu, C.-X. Wang, E. M. Aggoune, M. M. Alwakeel, and X.-H. You, "A general 3-D non-stationary 5G wireless channel model," *IEEE Trans. Commun.*, vol. 66, no. 7, pp. 3065–3078, Jul. 2018.
- [12] C.-X. Wang, J. Bian, J. Sun, W. Zhang, and M. Zhang, "A survey of 5G channel measurements and models," *IEEE Commun. Surveys Tuts.*, vol. 20, no. 4, pp. 3142–3168, 4th Quart. 2018.
- [13] "Final acts WRC-15: World radiocommunication conference," Int. Telecommun. Union, Geneva, Switzerland, ITU-Recommendation Final Acts WRC-15, 2015. [Online]. Available: https://www.itu.int/dms_pub/itu-r/opb/act/R-ACT-WRC.12-2015-PDF-E.pdf
- [14] L. Chettri and R. Bera, "A comprehensive survey on Internet of Things (IoT) toward 5G wireless systems," *IEEE Internet Things J.*, vol. 7, no. 1, pp. 16–22, Jan. 2020.
- [15] Y. Li, X. Cheng, Y. Cao, D. Wang, and L. Yang, "Smart choice for the smart grid: Narrowband Internet of Things (NB-IoT)," *IEEE Internet Things J.*, vol. 5, no. 3, pp. 1505–1515, Jun. 2018.
- [16] Y. Ran, "Considerations and suggestions on improvement of communication network disaster countermeasures after the Wenchuan earthquake," *IEEE Commun. Mag.*, vol. 49, no. 1, pp. 44–47, Jan. 2011.
- [17] D. Gomez-Barquero and M. W. Caldwell, "Broadcast television spectrum incentive auctions in the U.S.: Trends, challenges, and opportunities," *IEEE Commun. Mag.*, vol. 53, no. 7, pp. 50–56, Jul. 2015.
- [18] M. Park, "IEEE 802.11ah: Sub-1-GHz license-exempt operation for the Internet of Things," *IEEE Commun. Mag.*, vol. 53, no. 9, pp. 145–151, Sep. 2015.
- [19] A. Bishnu and V. Bhatia, "Receiver for IEEE 802.11ah in interference limited environments," *IEEE Internet Things J.*, vol. 5, no. 5, pp. 4109–4118, Oct. 2018.
- [20] K. Shah *et al.*, "Smart grid standards for operation in sub-1 GHz bands—An IEEE white paper," IEEE, Piscataway, NJ, USA, White Paper, Nov. 2018.
- [21] (2020). *GSMA 5G Spectrum*. [Online]. Available: <https://www.gsma.com/spectrum/wp-content/uploads/2018/11/5G-Spectrum-Positions.pdf>
- [22] C. R. Garcia, A. Lehner, T. Strang, and K. Frank, "Channel model for train to train communication using the 400 MHz band," in *Proc. IEEE Veh. Technol. Conf. (VTC-Spring)*, Singapore, May 2008, pp. 3082–3086.
- [23] R. Sevlian, C. Chun, I. Tan, A. Bahai, and K. Laberteaux, "Channel characterization for 700 MHz DSRC vehicular communication," *J. Elect. Comput. Eng.*, vol. 2010, pp. 1–9, Aug. 2010.
- [24] H. Fernández, L. Rubio, V. M. Rodrigo-Peñarrocha, and J. Reig, "Path loss characterization for vehicular communications at 700 MHz and 5.9 GHz under LOS and NLOS conditions," *IEEE Antennas Wireless Propag. Lett.*, vol. 13, pp. 931–934, 2014.
- [25] M. Zhu, G. Eriksson, and F. Tufvesson, "The COST 2100 channel model: Parameterization and validation based on outdoor MIMO measurements at 300 MHz," *IEEE Trans. Wireless Commun.*, vol. 12, no. 2, pp. 888–897, Feb. 2013.
- [26] H. W. Pflug *et al.*, "Radio channel characterization for 400 MHz implanted devices," in *Proc. IEEE Wireless Commun. Netw. Conf. (WCNC)*, Istanbul, Turkey, May 2014, pp. 293–298.
- [27] E. Bedeer, J. Pugh, C. Brown, and H. Yanikomeroglu, "Measurement-based path loss and delay spread propagation models in VHF/UHF bands for IoT communications," in *Proc. IEEE 86th Veh. Technol. Conf. (VTC-Fall)*, Toronto, ON, Canada, Sep. 2017, pp. 1–5.
- [28] K. Guan, Z. Zhong, B. Ai, and T. Kürner, "Propagation measurements and analysis for train stations of high-speed railway at 930 MHz," *IEEE Trans. Veh. Technol.*, vol. 63, no. 8, pp. 3499–3516, Oct. 2014.
- [29] C. K. Stoumpos and M. T. Chryssomallis, "Improvement of channel models performance with parameters values from measurements: A test case for suburban and rural environments at 450 MHz," *IEEE Antennas Wireless Propag. Lett.*, vol. 17, pp. 1396–1400, 2018.
- [30] H. Ozawa, T. Fujimoto, and M. Katayama, "Modeling of sub-GHz wave propagation in factories for reliable wireless communication," in *Proc. IEEE Int. Conf. Ind. Technol. (ICIT)*, Lyon, France, Feb. 2018, pp. 1598–1603.
- [31] P. Van Torre, J. Gaelens, J. Verhaevert, and H. Rogier, "Measurement and characterization of dual-band LoRa communication in the Antarctic," in *Proc. 12th Eur. Conf. Antennas Propag. (EuCAP)*, London, U.K., Apr. 2018, pp. 1–5.
- [32] M. Ohta, K. Adachi, N. Aihara, O. Takyu, T. Fujii, and M. Taromaru, "Measurement experiments on 920 MHz band for spectrum sharing with LoRaWAN," in *Proc. IEEE 88th Veh. Technol. Conf. (VTC-Fall)*, Chicago, IL, USA, Aug. 2018, pp. 1–5.
- [33] P. Van Torre, T. Ameloot, and H. Rogier, "Long-range body-to-body LoRa link at 868 MHz," in *Proc. 13th Eur. Conf. Antennas Propag. (EuCAP)*, Krakow, Poland, Apr. 2019, pp. 1–5.
- [34] J. Huang, C.-X. Wang, H. Chang, J. Sun, and X. Gao, "Multi-frequency multi-scenario millimeter wave MIMO channel measurements and modeling for B5G wireless communication systems," *IEEE J. Sel. Areas Commun.*, vol. 38, no. 9, pp. 2010–2025, Sep. 2020.
- [35] P. Kyosti *et al.*, *WINNER II Channel Models, WINNER II D1.1.2 V1.2*, document WINNER II Project, Apr. 2008.
- [36] "Study on 3D channel model for LTE (release 12), v12.2.0," 3GPP, Sophia Antipolis, France, 3GPP Rep. TR 36.873, Jun. 2015.
- [37] "Guidelines for evaluation of radio interface technologies for IMT-advanced," Int. Telecommun. Union, Geneva, Switzerland, ITU-Recommendation M.2135-1, Dec. 2009.



Jie Huang (Member, IEEE) received the B.E. degree in information engineering from Xidian University, Xi'an, China, in 2013, and the Ph.D. degree in information and communication engineering from Shandong University, Jinan, China, in 2018.

From October 2018 to October 2020, he was a Postdoctoral Research Associate with the National Mobile Communications Research Laboratory, Southeast University, Nanjing, China, supported by the National Postdoctoral Program for Innovative Talents. From January 2019 to February 2020, he was a Postdoctoral Research Associate with Durham University, Durham, U.K. Since March 2019, he has been a part-time researcher with Purple Mountain Laboratories, Nanjing. He is currently a Lecturer with the National Mobile Communications Research Laboratory, School of Information Science and Engineering, Southeast University. His research interests include millimeter wave, massive MIMO, intelligent reflecting surface channel measurements and modeling, wireless big data, and B5G/6G wireless communications.

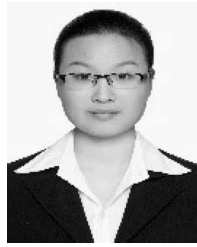
Dr. Huang received the Best Paper Awards from WPMC 2016 and WCSP 2020.



Cheng-Xiang Wang (Fellow, IEEE) received the B.Sc. and M.Eng. degrees in communication and information systems from Shandong University, Jinan, China, in 1997 and 2000, respectively, and the Ph.D. degree in wireless communications from Aalborg University, Aalborg, Denmark, in 2004.

He was a Research Assistant with the Hamburg University of Technology, Hamburg, Germany, from 2000 to 2001, a Visiting Researcher with Siemens AG Mobile Phones, Munich, Germany, in 2004, and a Research Fellow with the University of Agder, Grimstad, Norway, from 2001 to 2005. He has been with Heriot-Watt University, Edinburgh, U.K., since 2005, where he was promoted to a Professor in 2011. In 2018, he joined Southeast University, Nanjing, China, as a Professor. He is also a part-time Professor with the Purple Mountain Laboratories, Nanjing. He has authored four books, two book chapters, and more than 400 papers in refereed journals and conference proceedings, including 24 Highly Cited Papers. He has also delivered 22 Invited Keynote Speeches/Talks and seven Tutorials in international conferences. His current research interests include wireless channel measurements and modeling, B5G wireless communication networks, and applying artificial intelligence to wireless communication networks.

Prof. Wang received twelve Best Paper Awards from IEEE GLOBECOM 2010, IEEE ICCT 2011, ITST 2012, IEEE VTC 2013-Spring, IWCMC 2015, IWCMC 2016, IEEE/CIC ICC 2016, WPMC 2016, WCCC 2019, IWCMC 2020, and WCSP 2020. He is currently an Executive Editorial Committee member for the IEEE TRANSACTIONS ON WIRELESS COMMUNICATIONS. He has served as an Editor for nine international journals, including the IEEE TRANSACTIONS ON WIRELESS COMMUNICATIONS from 2007 to 2009, the IEEE TRANSACTIONS ON VEHICULAR TECHNOLOGY from 2011 to 2017, and the IEEE TRANSACTIONS ON COMMUNICATIONS from 2015 to 2017. He was a Guest Editor of the IEEE JOURNAL ON SELECTED AREAS IN COMMUNICATIONS, Special Issue on Vehicular Communications and Networks (Lead Guest Editor), Special Issue on Spectrum and Energy Efficient Design of Wireless Communication Networks, and Special Issue on Airborne Communication Networks. He was also a Guest Editor of the IEEE TRANSACTIONS ON BIG DATA, Special Issue on Wireless Big Data, and is a Guest Editor for the IEEE TRANSACTIONS ON COGNITIVE COMMUNICATIONS AND NETWORKING, Special Issue on Intelligent Resource Management for 5G and Beyond. He has served as a TPC Member, TPC Chair, and General Chair for over 80 international conferences. He is a Fellow of the IET, a member of the Academia Europaea, an IEEE Communications Society Distinguished Lecturer in 2019 and 2020, and a Highly Cited Researcher recognized by Clarivate Analytics, in 2017–2020.



Yuqian Yang received the M.Sc. degree from the School of Information Science and Engineering, Shandong University, Qingdao, China, in 2019.

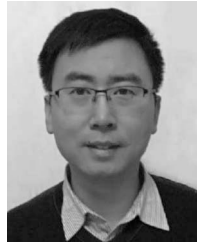
She is currently working as an NPO Junior Engineer with China Mobile, Zhejiang, China. She is currently concentrating on industry application of 5G technology and network slicing technology.



Yu Liu (Member, IEEE) received the Ph.D. degree in communication and information systems from Shandong University, Jinan, China, in 2017.

From 2015 to 2017, she was a Visiting Scholar with the School of Engineering and Physical Sciences, Heriot-Watt University, Edinburgh, U.K. From 2017 to 2019, she was a Postdoctoral Research Associate with the School of Information Science and Engineering, Shandong University. Since 2019, she has been an Associate Professor with the School of Microelectronics, Shandong University. Her main

research interests include nonstationary wireless MIMO channel modeling, high speed train wireless propagation characterization and modeling, and channel modeling for special scenarios.



Jian Sun (Member, IEEE) received the B.Sc. degree in applied electronic technology, the M.Eng. degree in measuring and testing technologies and instruments, and the Ph.D. degree in communication and information systems from Zhejiang University, Hangzhou, China, in 1996, 1999, and 2005, respectively.

From 2005 to 2018, he was a Lecturer with the School of Information Science and Engineering, Shandong University, Jinan, China, where he has been an Associate Professor since 2018. In 2008, he was a Visiting Scholar with the University of California at San Diego, San Diego, CA, USA. In 2011, he was a Visiting Scholar with Heriot-Watt University, Edinburgh, U.K., supported by U.K.-China Science Bridges: Research and Development on B4G Wireless Mobile Communications project. His current research interests include signal processing for wireless communications, channel sounding and modeling, propagation measurement and parameter extraction, maritime communication, visible light communication, software-defined radio, MIMO, multicarrier, and wireless systems design and implementation.



Wensheng Zhang (Member, IEEE) received the M.E. degree in electrical engineering from Shandong University, Qingdao, China, in 2005, and the Ph.D. degree in electrical engineering from Keio University, Tokyo, Japan, in 2011.

In 2011, he joined the School of Information Science and Engineering, Shandong University, where he is currently an Associate Professor. He was a Visiting Scholar with the University of Oulu, Oulu, Finland, in 2010 and University of Arkansas, Fayetteville, AR, USA, in 2019. His research interests lie in tensor computing, random matrix theory, and intelligent B5G wireless communications.